Received: 9 July 2020 | Revised: 15 March 2021 | Accepted: 15 March 2021

DOI: 10.1002/joc.7101

RESEARCH ARTICLE

International Journal of Climatology RMetS

Seasonal distribution and variability of surface winds in the Indonesian seas using scatterometer and reanalysis data

Inovasita Alifdini[1] | **Teruhisa Shimada**[1] | **Anindya Wirasatriya**[2,3]

[1]Graduate School of Science and Technology, Hirosaki University, Hirosaki, Japan

[2]Oceanography Department, Faculty of Fisheries and Marine Sciences, Diponegoro University, Semarang, Indonesia

[3]Center for Coastal Rehabilitation and Disaster Mitigation Studies, Diponegoro University, Semarang, Indonesia

Correspondence
Inovasita Alifdini, Graduate School of Science and Technology, Hirosaki University, Hirosaki, Japan.
Email: inovasita@gmail.com

Abstract

The distribution and variability of surface winds in the seas and straits in the Maritime Continent, or the Indonesian seas, are investigated using scatterometer wind measurements and reanalysis wind data. This study focuses on the detailed climatology of surface winds in the Indonesian seas and has significant implications for a better understanding of regional climate, meteorological disasters, and offshore wind resource. The monsoon winds predominantly blow over the seas along the routes formed by the coastlines of the large islands and the chains of the small islands. The wind speeds are persistently strong along these routes, and the major direction of the variability in winds is well aligned with these routes. The wind jets are formed in the central part of the routes. The interisland gaps and channels form wind jets of various scales. The Australian winter monsoon is stronger and more persistent than the East Asian winter monsoon in the Indonesian seas. The onset of each monsoon differs by approximately 40 days between the east and west of the Indonesian seas. The amplitudes and spatial extents of diurnally varying winds dominate along the northern coasts of Java Island and the small islands to the east, along the northwest and northeast coasts of Borneo, along the coast of southern Sulawesi Island, and to the southwest of Papua, and vanish along the centre lines of the monsoon routes. Sea areas with a large amplitude of diurnally varying wind are much the same throughout the year. The amplitude of diurnally varying wind has an annual maximum in September in the southern Indonesian seas, possibly in correspondence with the annual maximum of the temperature difference between land and sea.

KEYWORDS

Australian winter monsoon, diurnally varying wind, East Asian winter monsoon, Indonesian seas, Maritime Continent, sea surface wind, wind climatology

1 | INTRODUCTION

In the Maritime Continent, the East Asian winter monsoon dominates in December–March, and the Australian winter monsoon dominates in May–October (Aldrian and Susanto, 2003; Ronghui *et al.*, 2004; Wang *et al.*, 2010). The two monsoons reverse seasonally and undergo a transition in April and November. The wind induced by the Asian–Australian monsoon system blows throughout the Maritime Continent, which comprises islands of various sizes and heights and seas connected to straits (Figure 1a). The small seas and straits within the Maritime Continent

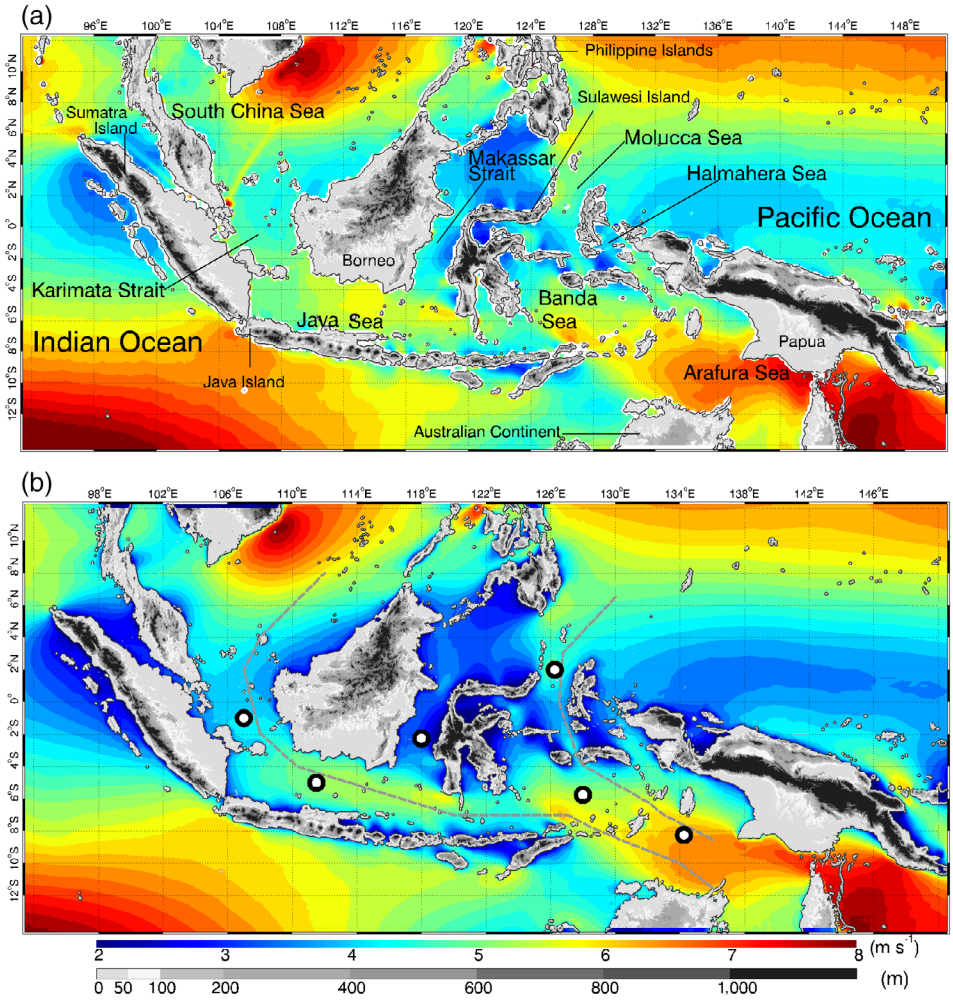

FIGURE 1 Annual averages of wind speed derived from (a) ASCAT and (b) hourly data of ERA5 at 10 m (colour shading). The grayscale shading in these maps and the other map figures show topographic elevation. The geographical names referred to in this paper are shown in (a). Black-and-white points at sea in (b) are the six selected locations for the subsequent analyses. The dashed grey lines in (b) show the defined routes for the analysis in Figure 10 [Colour figure can be viewed at wileyonlinelibrary.com]

are collectively referred to as the Indonesian seas. The monsoon wind is a key factor influencing the regional climate. In the Indonesian seas, the monsoon winds influence regional oceanographic conditions. The along-shore winds induce coastal upwelling owing to seaward Ekman transport (Susanto *et al*., 2006; Iskandar *et al*., 2009). The seasonally reversing monsoon winds change the volume transport of the Indonesian Throughflow (Xu, 2014; Sprintall *et al*., 2019). The variability in the monsoon system is induced by global climate systems, such as the El Niño Southern Oscillation (ENSO; Xu and Chan, 2001; Meehl and Arblaster, 2011) and the Indian Ocean Dipole (IOD; Jourdain *et al*., 2013), and the Madden–Julian Oscillation (MJO; Zhang, 2013). Currently, studies on winds in the Indonesian seas have attracted increasing attention in the development of offshore wind energy (Hasan *et al*., 2012; Gernaat *et al*., 2014; Ahmed *et al*., 2017; EMD International A/S, 2017). Thus, understanding the winds over the seas of the Maritime Continent or the Indonesian seas has been a long-standing challenge and of increasing importance.

Distributions and temporal variations of surface winds in specific regions have been investigated using satellite scatterometers or satellite-based wind data. The QuikSCAT wind data are used to examine the winds in the Java Sea (Hattori *et al*., 2011), the Makassar Strait (Gordon *et al*., 2003; Susanto *et al*., 2012), the seas around Sulawesi and Molucca Islands (Mahmuddin and Hamzah, 2015), and the Halmahera Sea (Setiawan *et al*., 2019). Wirasatriya *et al*. (2019) show the surface winds in the northern Molucca Sea using the cross-calibrated multiplatform (CCMP) data. Lang (2017) investigates the winds in the seas around the Philippine Islands using the RapidScat and CCMP data. The monsoon winds in the lower atmosphere over the Indonesian seas are examined in terms of large-scale atmospheric circulation using atmospheric reanalysis data (e.g., Juneng and Tangang, 2005; Chang *et al*., 2005a; Jiang *et al*., 2019). In addition, the diurnal cycle of wind has been discussed within the context of the diurnal cycle of precipitation in the Indonesian seas (e.g., Ichikawa and Yasunari, 2006; Qian *et al*., 2010, 2013; Bhatt *et al*., 2016;

Vincent and Lane, 2017). Short *et al*. (2019) showed that the diurnal cycle of surface winds significantly contributes to the formation of precipitation over the islands and surrounding seas. Araki *et al*. (2006) investigated seasonal and interannual variations in the diurnal cycle of wind in Serpong, Indonesia. In the Java Sea, the diurnal cycle of wind is modified by fluctuations of the East Asian winter monsoon owing to the tongue-shaped cold water in the South China Sea (Koseki *et al*., 2013).

However, the results of the aforementioned studies are limited to specific seasons or specific regions of the Indonesian seas. Although a considerable number of studies have been conducted on meteorology and climate in the Maritime Continent, their principal objectives are the role of the Maritime Continent in large-scale meteorology and climate. Only a few studies specifically focus on the low-level winds in the Indonesian seas, where many islands and seas form complicated topography and land-sea contrast. The current understanding of the low-level winds is inadequate for many practical applications. For example, the wind from the surface up to 150 m is important for the development of offshore wind energy. The topographic effects exert particularly strong influences on the surface wind field. Observations of the surface winds are relatively accessible and observational evidences of the surface winds are an important indicator of the low-level winds. Nonetheless, wind climatology in the Indonesian seas remains an open question. Thus, the following three challenges need to be addressed. Firstly, few studies have investigated the detailed distributions of wind in the Indonesian seas. The focus must be placed on the wind in the Indonesian seas to characterize the wind distribution and to examine the topographic effects of the islands on the wind. Identifying key locations where strong and persistent wind occurs is also useful for statistical analyses. Secondly, the complicated topography of the islands in the Indonesian seas exerts a significant influence on the variability of the monsoon winds. Accordingly, it is necessary to examine the variability in surface winds associated with the Asian–Australian monsoon system. Thirdly, the diurnal variations of wind have been examined mainly in the vicinity of the islands. The seasonal and regional changes of the spatial extent and the strength of diurnally varying winds resulting from the complicated land-sea contrast must be investigated. These challenges have not been addressed in the previous studies, because few studies have attempted to obtain a comprehensive picture of surface winds in the Indonesian seas. Therefore, in this study, we investigate the surface winds in the Indonesian seas using satellite observations and reanalysis data. We focus on the Indonesian seas or the inner seas in the Maritime Continent, bounded by the Pacific Ocean, the Indian Ocean, and the South China Sea (Figure 1a), to provide further insights into the detailed structures of surface winds and regional differences in wind variability.

Section 2 provides an overview of the data and methods used in this study. In section 3, we present the distribution of surface winds and the key locations selected for the subsequent analyses. Section 4 describes the variability in surface winds associated with the Asian–Australian monsoon system. Section 5 explores the diurnal variations in surface winds. Section 6 presents a summary and conclusions.

2 | DATA AND METHODS

We used wind measurements by the Advanced SCATterometer (ASCAT) onboard Meteorological Operational-A (MetOp-A) and Meteorological Operational-B (MetOp-B) satellites at a sampling resolution of 12.5 km for 2010–2018 (EUMETSAT/OSI SAF, 2010, 2013). The near-real-time datasets common to ASCAT/MetOp-A and ASCAT/MetOp-B are consistently used, which is available from 2010. The ASCAT datasets provide observational evidence of surface winds in the island-studded seas. The MetOp-A and -B satellites cross the equator at 09:30 (local solar time) on the descending node and at 21:30 (local solar time) on the ascending node. We used approximately 3,100 swath data over the Maritime Continent per year for each satellite to derive gridded data with a 0.125°×0.125° interval by applying the land presence flag to remove low quality data near the coast. The land presence flag is set if some portion of a wind vector cell includes land. The ASCAT operates in the C-band, which is less sensitive to rain than Ku-band scatterometers, such as QuikSCAT (Figa-Saldaña *et al*., 2002). The ASCAT wind product showed the highest accuracy in both wind speed and direction and have the least error statistics compared to other scatterometers data (i.e., OSCAT and HY-2A SCAT; Wu and Chen, 2015). Kumar *et al*. (2019) showed that both ASCAT datasets have a negligible bias (0.14 m s^{-1} for ASCAT/MetOp-A and 0.20 m s^{-1} for ASCAT/MetOp-B) by comparing to the observations acquired by the buoys in the Indian Ocean. The results derived from the ASCAT data in this study are based on the 9-year data.

We analysed hourly winds at a height of 10 m from the fifth-generation atmospheric reanalysis ERA5 provided by the European Centre for Medium-Range Weather Forecasts (ECMWF) at a spatial grid of 0.25° for 2010–2018 (Copernicus Climate Change Service [C3S], 2017; Hersbach *et al*., 2020). The ERA5 wind data at a height of 100 m are used for comparison with the wind fields at a height of 10 m. Skin temperature data were also used to derive land and sea surface

temperatures. Previous studies discussed the accuracy of ERA5 wind and skin temperature data. Rivas and Stoffelen (2019) showed systematic differences in the mean zonal winds of ERA5 in the tropics up to 0.5 m s^{-1} relative to ASCAT. However, the use of the ERA5 wind data is an effective approach because the ERA5 wind data shows a 20% improvement relative to the ERA-Interim wind data (Rivas and Stoffelen, 2019) and because the ERA5 data show the best estimation of surface wind compared with the other five reanalysis data (Ramon *et al*., 2019). Luo and Minnett (2020) validated the ERA5 sea skin temperature dataset with ship-based radiometric measurements and showed that these two datasets have a high correlation of .993, with an average bias of −0.213 K relative to the ship-based radiometric measurements. These results indicate the applicability of the ERA5 data for climate analyses in the tropics. The latest reanalysis data of ERA5 with high spatiotemporal grid resolution enable the effective analyses of the wind distribution in the Indonesian seas and of the diurnally varying wind. The results derived from ERA5 in this study are based on the 9-year data.

To examine the consistency between the ERA5 data and in situ data, we used wind data acquired at observation stations on the Indonesian islands, which are obtained from the National Centers for Environmental Information (NCEI) of the National Oceanic and Atmospheric Administration (NOAA). Furthermore, we used hourly wind data from four Triangle Trans-Ocean Buoy Network (TRITON) buoys located in the north Papua, which are obtained from the Pacific Marine Environmental Laboratory (PMEL) of the NOAA for the same data period as the ERA5. The wind speeds acquired at a height of 4 m are converted to those at a height of 10 m using the COARE Bulk algorithm (Fairall *et al*., 1996).

To analyse the variability in wind, we used a principal component analysis method. We computed velocity variance ellipses and eddy kinetic energy following the method of Chelton *et al*. (2000) and Shimada (2010). The principal axes of variance in wind are derived from the eigenvalues and eigenvectors of the covariance matrix of the data at a given location. The eddy kinetic energy is a mean of eigenvalues. For example, the highly anisotropic velocity variance ellipses accompanied by large eddy kinetic energy indicate high wind variability in a particular direction. This analysis method is useful in regions where the winds are influenced by topography.

To show the regional differences in the diurnally varying wind, the vector anomaly of hourly wind is calculated by subtracting daily vector average wind from hourly vector average wind. Then, we defined the diurnal amplitude as the mean magnitude of 24 wind vector anomalies for every hour. In addition, we computed monthly means of daily maxima of the surface temperature difference between land and sea. This temperature difference is derived by subtracting the monthly mean of hourly sea surface temperature from the monthly mean of hourly land surface temperature for each grid in the defined regions.

3 | DISTRIBUTION AND KEY LOCATIONS

The annual mean of the scalar wind speed in the Indonesian seas using the ASCAT wind measurements is depicted in Figure 1a. The Indonesian seas are surrounded by three regions (the South China Sea, the Pacific Ocean, and the Indian Ocean) with mean wind speeds typically greater than 5 m s^{-1} (Chang *et al*., 2005b; Wang *et al*., 2010; Koseki *et al*., 2013). In the Indonesian seas, high wind speeds comparable to those in open oceans are apparent. High wind speeds exceeding 6 m s^{-1} are observed in the Arafura Sea and the Banda Sea. Localized high wind speeds are observed in the Java Sea. On the other hand, the mean wind speeds are relatively low in the Molucca Sea, Halmahera Sea, Karimata Strait, Makassar Strait, and especially to the north of Sulawesi Island, possibly owing to the topographic blockage. These features are consistently confirmed in the corresponding map derived from the ERA5 data (Figure 1b). The wind speed in ERA5 exhibits a lower speed than in ASCAT in most of the Indonesian seas. The spatial correlation between these wind fields is .94 and the root mean square error is 0.71 m s^{-1}, although the bias is negative (−0.52 m s^{-1}) especially for speeds less than 4 m s^{-1} (Figure S1a). Thus, the wind speeds in the Indonesian seas have large spatial variability.

To distinguish the features seen in Figure 1, we illustrate the monthly means of vector winds in January (Figure 2) and August (Figure 3). These two months correspond to the peak periods of the East Asian winter monsoon and the Australian winter monsoon, respectively, and the wind fields in these two months are representative of those during the respective monsoons. In January, the wind associated with the East Asian winter monsoon blows into the Indonesian seas from the South China Sea towards the Arafura Sea via the Karimata Strait, the Java Sea, and the Banda Sea, with speeds exceeding 5 m s^{-1} (Figure 2). This wind flow is clearly distinguished from the ambient winds. The moderately strong winds extending from the trade wind region in the Pacific Ocean blow through the Molucca Sea to the Banda Sea, merging into the wind flow originating from the South China Sea. In August, the southeasterly wind with speeds exceeding 6 m s^{-1} blows mainly through two

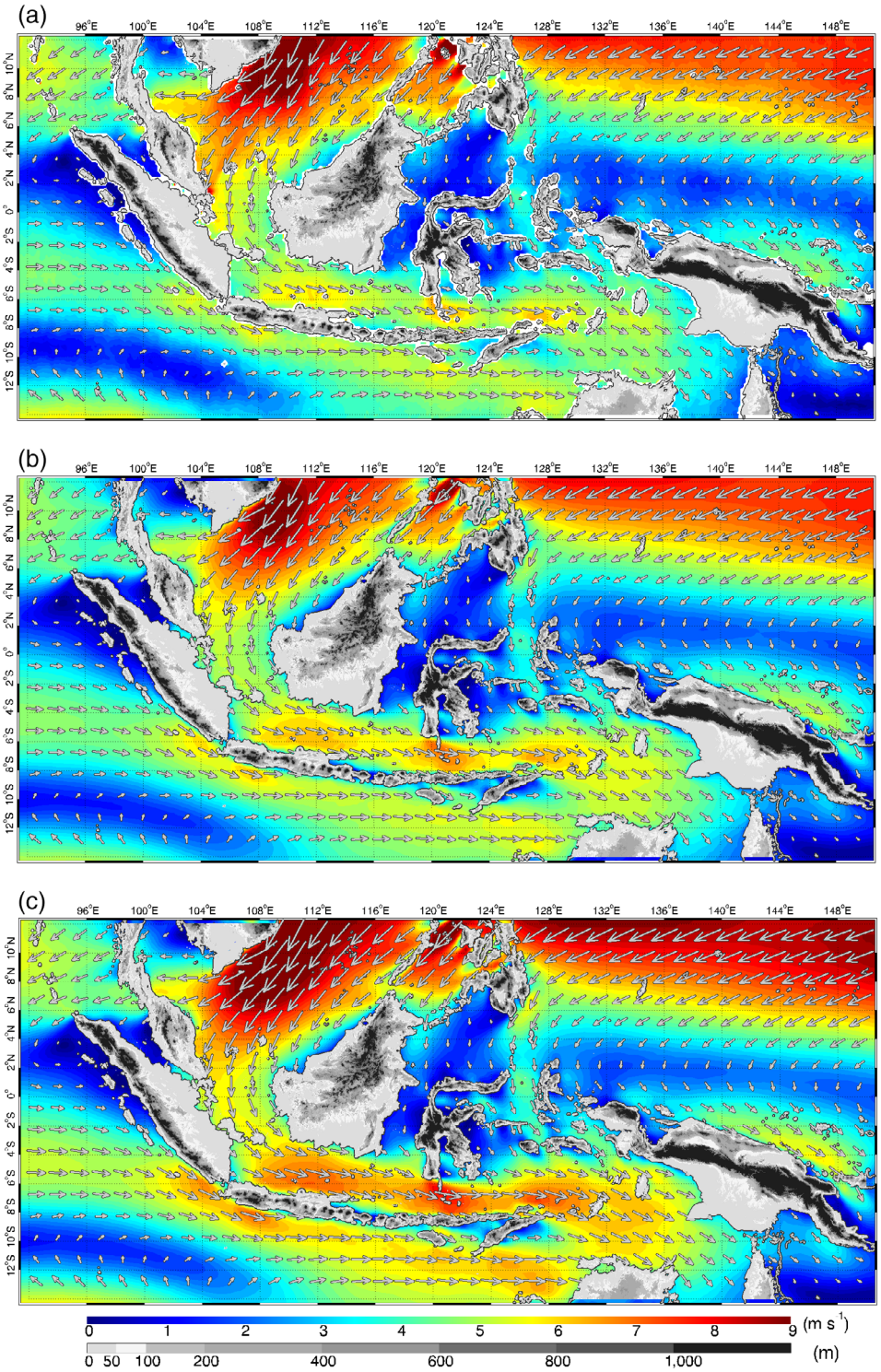

FIGURE 2 Monthly means of wind vectors in January from (a) ASCAT, (b) hourly data of ERA5 at 10 m, and (c) hourly data of ERA5 at 100 m. The colour shading shows wind speed. The vectors are plotted at every 12 grid points in (a) and at every 6 grid points in (b, c) or 1.5° × 1.5°, for clarity [Colour figure can be viewed at wileyonlinelibrary.com]

routes in the Indonesian seas (Figure 3). One route extends from the Arafura Sea to the south of the Philippine Islands or the Pacific Ocean through the Molucca Sea and the Halmahera Sea. Winds are intensified in the Molucca Sea and the Halmahera Sea when passing between the islands, and these strong winds are in contrast to the weak winds in the lee of Sulawesi Island and Papua Island. The other route bifurcates from the Banda Sea and extends to the Karimata Strait through the Java Sea, reaching the South China Sea. Moderate wind speeds (3–4 m s^{-1}) are observed in the Makassar Strait, suggesting a wind route from south to north in August. The distributions of surface winds derived from the ERA5 data in Figures 2b and 3b are consistent with

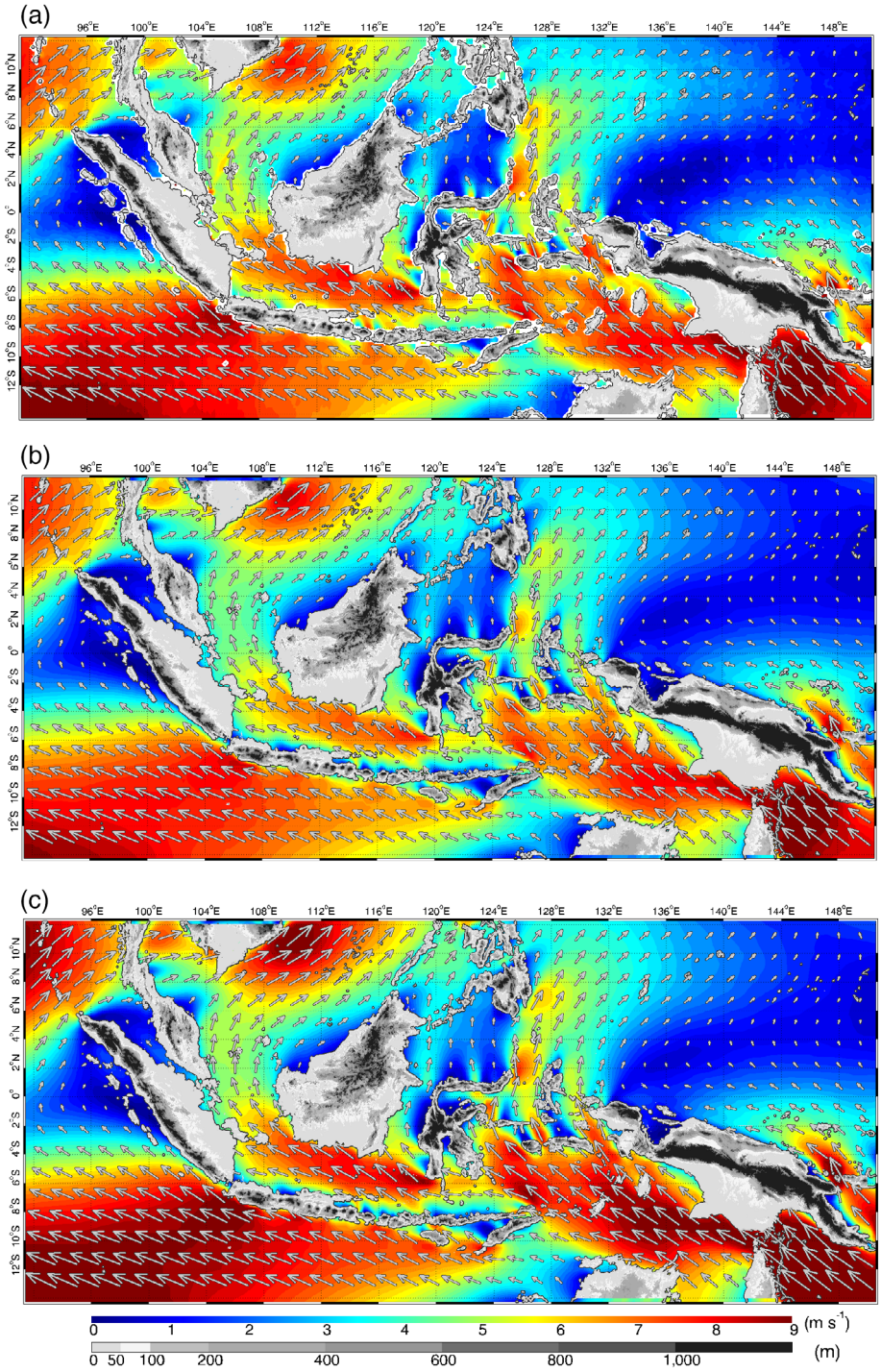

FIGURE 3 The same as Figure 2 but in August [Colour figure can be viewed at wileyonlinelibrary.com]

those derived from the ASCAT data in Figures 2a and 3a, although the differences in speeds are slightly larger in the Java Sea. The mean bias is −0.15 m s^{-1}, the root mean square error is 0.74 m s^{-1}, and the correlation is .94 from the comparison of wind speed derived from vector average winds between ASCAT and ERA5 (Figure S1b). Thus, from these results, it is established that the Indonesian seas provide important routes of the monsoon wind.

We here explore the monthly means of vector winds at 100 m from the ERA5 data (Figures 2c and 3c). The distribution or spatial contrast of the wind fields at a height of 100 m is consistent with that at a height of 10 m. While the differences in wind speeds between 10 m and 100 m increase with speed, the relationship of wind speeds between 10 and 100 m are evident (Figure 4a,c), in spite of possible regional differences in stratification. The wind directions are consistent between 10 and 100 m (Figure 4b,

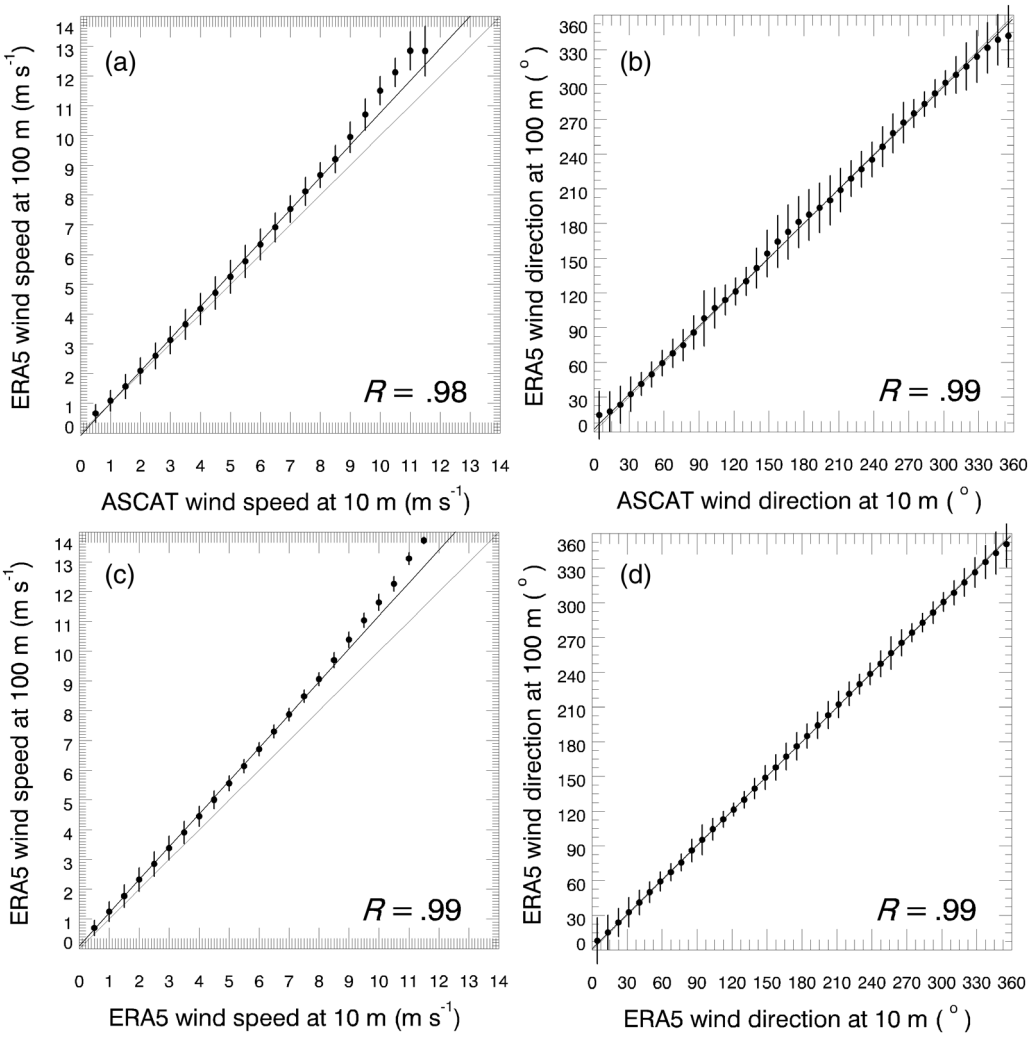

FIGURE 4 Binned scatterplots of (a,c) wind speeds and (b,d) wind directions between 10 m and 100 m. In (a,b), wind speed and direction between ASCAT and ERA5 are compared, and in (c,d), ERA5 10 m and 100 m wind data are compared. The dots are the means within each bin, and the error bars (vertical lines) are the plus or minus one standard deviation within each bin. The data are extracted from the monthly means of wind vectors from January to December covering the Indonesian seas (14°S–12°N, 92°–150°E) at a grid interval of 0.25° by excluding the data at land grid points. The thick line is the regression line, and R is the correlation coefficient. The ERA5 data plotted in this figure have the same time as ASCAT (number of samples is 219,732). The root mean square errors in (a–d) are the following: 0.55 m s^{-1}, 15.5°, 0.58 m s^{-1}, and 9.66°, respectively. The biases in (a–d) are 0.25 m s^{-1}, 0.34°, 0.44 m s^{-1}, and 0.06°, respectively

d). From these results, the wind routes with high wind speeds are clearly confirmed at a height of 100 m.

The monthly means of the wind curl reveal the fine structures of the wind fields (Figure 5). The wind curl is computed as $\nabla \times \mathbf{u}$ where $\mathbf{u}$ is the horizontal wind vector. A wind jet blowing from a mountain gap or a channel between islands is detected as a pair of positive and negative values of wind curl, and wind passing through the tip of an island or a peninsula is detected as a positive or negative value of wind curl (Chelton *et al*., 2004). In January, the positive and negative wind curl are respectively found along the northern and southern coasts of the Java Sea and the Banda Sea (Figure 5a). These structures indicate a large wind jet associated with the East Asian winter monsoon. The axis of the wind jet, which is represented by the zero line of the wind curl, is centrally located in the Java Sea and the Banda Sea. It is noteworthy that the jet structure is not detected in the Karimata Strait, while this strait is the major route of the East Asian winter monsoon. Only a positive wind curl appears when the monsoon blows into the Karimata Strait. In the Molucca Sea and the Banda Sea, small-scale structures of pairs of positive and negative wind curls indicate strong winds blowing through the channels between the islands. In August, a large wind jet associated with the Australian winter monsoon is indicated by the positive and negative wind curls along the southern and northern coasts of the Java Sea and the Banda Sea (Figure 5b). The interisland

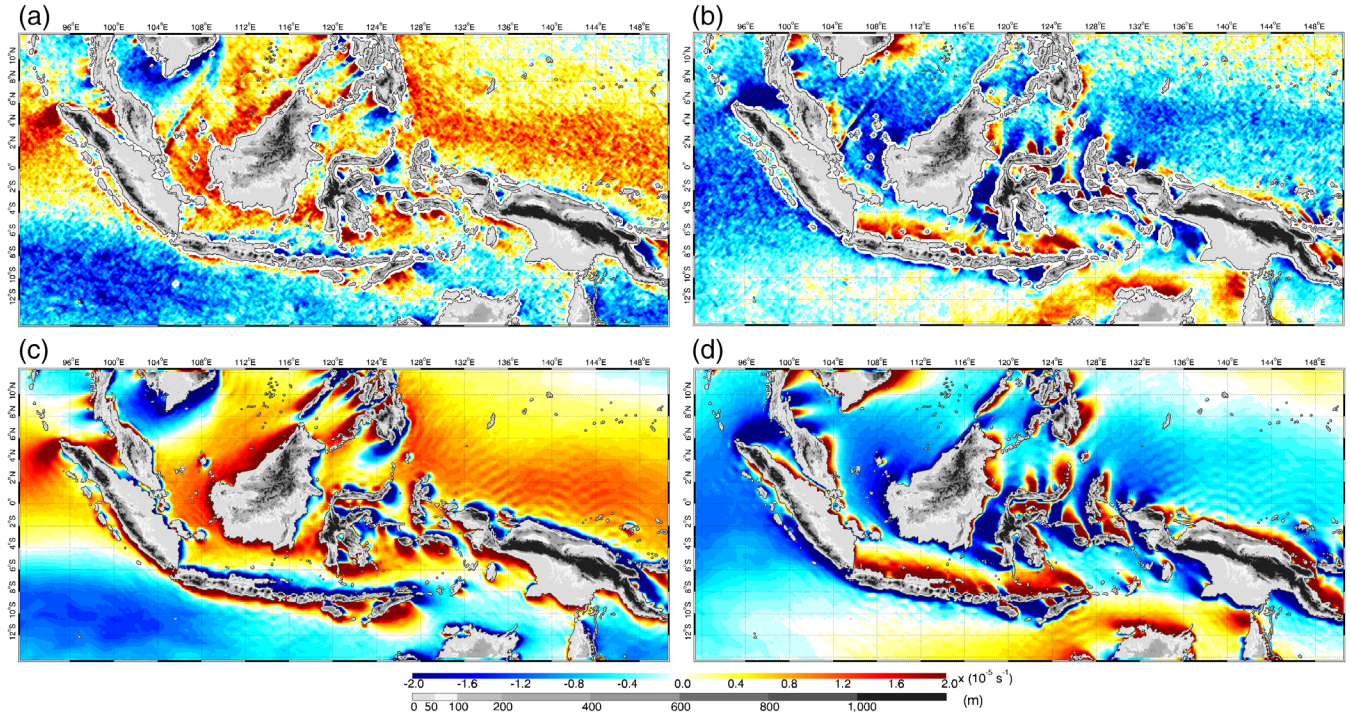

FIGURE 5 Monthly means of wind curl from (a,b) ASCAT and (c,d) hourly data of ERA5 at 10 m in (a,c) January and in (b,d) August [Colour figure can be viewed at wileyonlinelibrary.com]

gaps and channels form wind jets along the northern coast of Java Island and the islands to the east. In the Molucca Sea, the Halmahera Sea, and the Makassar Strait, multiple pairs of positive and negative wind curl are found. These structures indicate small-scale wind jets, inducing large spatial variability in sea surface winds owing to the islands. Along the southern coasts of Sumatra and Java Islands, the narrow bands of the positive and negative wind curl are seen in January and August, respectively, reflecting the drag effect on the strong winds blowing along the coasts. In the wind curl fields derived from the ERA5 data, these features are smoothed but recognizable (Figure 5c,d). The mean bias is -0.08×10^{-6} s^{-1}, the root mean square error is 9.95×10^{-6} s^{-1}, and the correlation is .81 (Figure S1c). Thus, we could shed light on the fine structures of wind in the entire Indonesian seas, which are blurred in the wind curl fields derived from the QuikSCAT wind data with a 25 km grid resolution and have not been focused on (Chelton *et al.*, 2004; Risien and Chelton, 2008).

From the results in Section 3, we chose the following six key locations on the routes of the monsoon winds for the subsequent analyses: the Karimata Strait (1.00°S/107.00°E), Java Sea (5.00°S/111.50°E), Banda Sea (5.75°S/128.00°E), Arafura Sea (8.25°S/134.25°E), Makassar Strait (2.25°S/118.00°E), and Molucca Sea (2.00°N/126.25°E; Figure 1b). The wind variability in these six locations can be representative of that in the surrounding seas. Although we mainly focus on the ASCAT wind measurements for investigating the spatial distribution of winds shown in Figures 1, 2, 3, and 5, we confirmed that the spatial grid size of the ERA5 data is enough to analyse the wind along the main monsoon routes. In this and subsequent sections, we discuss the general features of winds observed in both datasets.

4 | VARIABILITY ASSOCIATED WITH THE MONSOON SYSTEM

To examine the variability in wind, we computed variance ellipses and eddy kinetic energy in the Indonesian seas (Figure 6). The most remarkable feature is that the velocity variance ellipses are highly anisotropic in the Indonesian seas (Figure 6a). From the South China Sea to the Arafura Sea via the Karimata Strait, the Banda Sea, and the Arafura Sea, the major axes of the anisotropic velocity variance ellipses are well aligned with the coastlines of the large islands and the chains of the small islands. These seas are characterized by large eddy kinetic energy (>15 m^2 s^{-2}). The most anisotropic velocity variance ellipses and the largest eddy kinetic energy are distributed in the Arafura Sea and the South China Sea. In the Molucca Sea, Halmahera Sea, and Makassar Strait, the velocity variances are still weakly anisotropic, and the major axes of the velocity variances

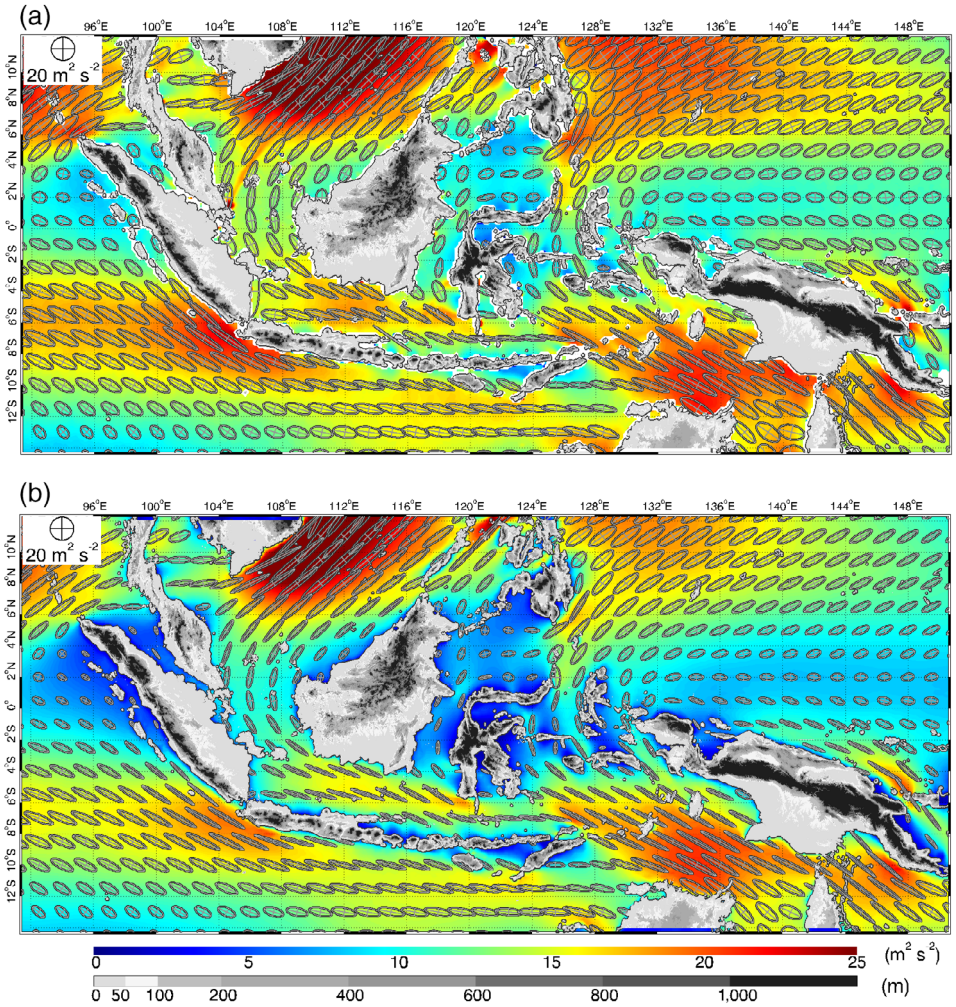

FIGURE 6 Maps of wind velocity variance ellipses (ellipses and crossed lines) and eddy kinetic energy per unit mass (colour shading). These maps are derived from (a) ASCAT and (b) hourly data of ERA5 at 10 m for all the months during 2010–2018. The ellipses are plotted at every 12 grid points in (a) and at every 6 grid points in (b) or 1.5° × 1.5°, for clarity [Colour figure can be viewed at wileyonlinelibrary.com]

are aligned with the mean wind direction in Figures 2 and 3. Thus, the strong wind regions shown in Figures 1, 2, and 3 are accompanied by highly anisotropic velocity variance ellipses and large eddy kinetic energy. The large eddy kinetic energy arises mainly from variability in the wind direction associated with the seasonal reversal of the monsoons. Figures 2, 3, and 6 indicate that the monsoon winds blow through the study region mostly over the seas along the routes formed by the coastline of the large islands and the chains of the small islands. We can confirm the anisotropic velocity variance ellipses and consistent distribution of the eddy kinetic energy from the ERA5 data, except that the eddy kinetic energy derived from the ERA5 data is lower than that derived from the ASCAT data, especially in the Karimata Strait, the Java Sea, and the seas around Sulawesi Island where the wind speeds of the ERA5 data are lower than those of the ASCAT data (Figure 6b). The spatial correlation of eddy kinetic energy between Figure 6a,b is .91, the root mean square error is 3.13 m^2 s^{-2}, and the mean bias is −2.39 m^2 s^{-2} (Figure S1d).

We confirm the variability of wind in the Indonesian seas from the annual wind roses in the selected six locations (Figure 7). The wind roses show the occurrence probability of wind direction for wind speeds less than a given threshold. All the wind roses show high directionality in two opposing directions. The directions of the two dominant peaks correspond to the directions of the coastlines formed by the large islands and the chains of the small islands around the respective locations. This result indicates that the wind direction associated with the monsoons is significantly stable. In the locations along the route ranging from the Karimata Strait to the Arafura Sea, the peak frequencies of wind direction associated with the Australian winter monsoon are more than twice those associated with the East Asian winter monsoon (Figure 7a,d–f). In the Makassar Strait and the Molucca Sea, the wind roses are slightly wider than the others because of the variable wind direction at low wind speeds (Figure 7b,c). The high directionality of the wind roses is also represented by the ERA5 data (Figure 7g–l), except that the variable winds associated

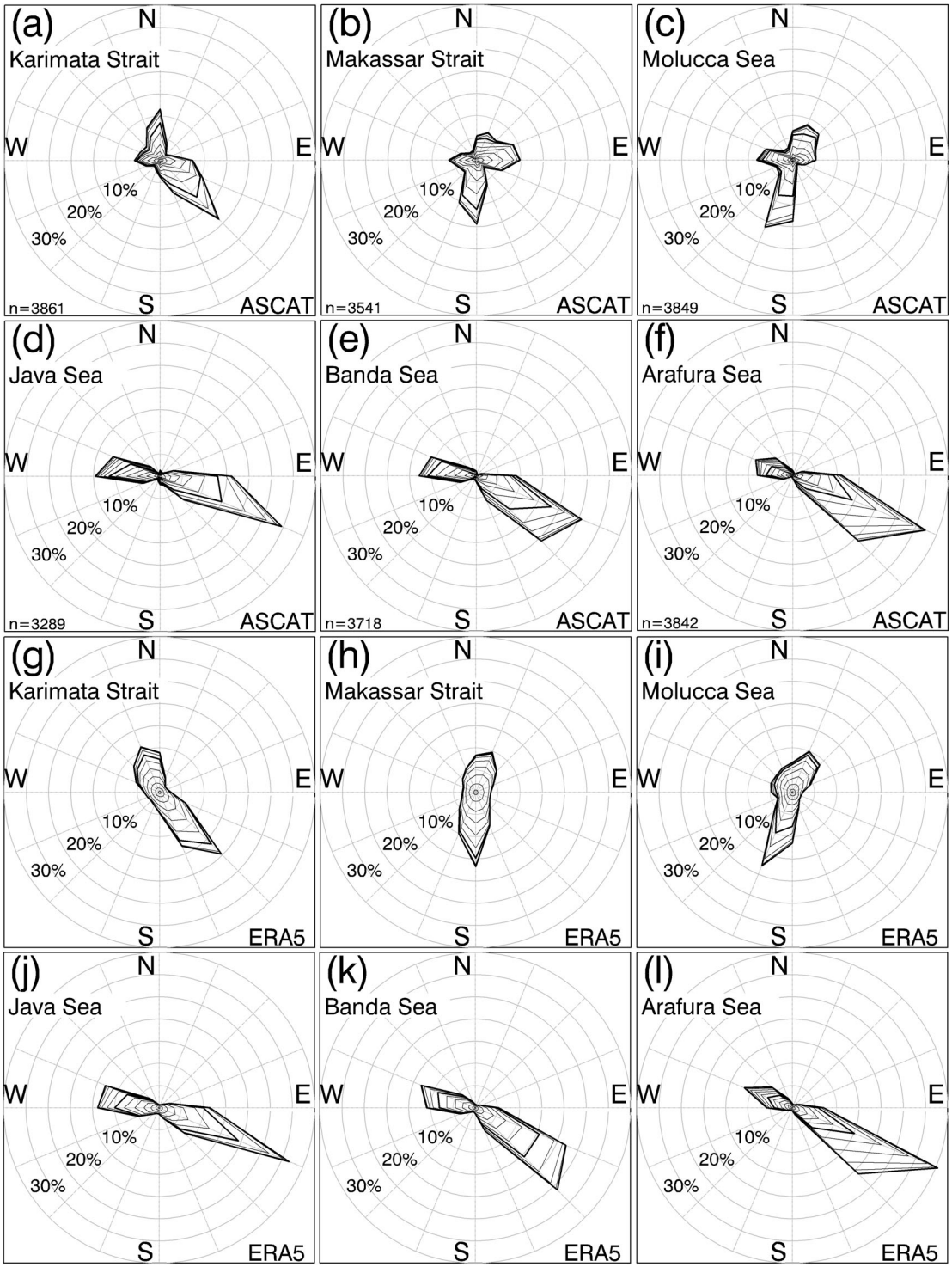

FIGURE 7 Annual wind roses composed of (a–f) ASCAT and (g–l) ERA5 hourly data at 10 m in the selected six locations shown in Figure 1b. Wind direction is defined as the direction from which the wind blows. The compass is divided into 16 sectors. The polygons show the cumulative relative frequency of wind direction with speeds less than a threshold speed for every 1 m s^{-1} (thin and bold contours). The bold polygons inside are composed of the data with speeds less than 7 m s^{-1} and the bold outermost polygons are composed of all the data. The circles are the isolines of the cumulative relative frequency of wind direction in the range from 5 to 35%. The numbers of ASCAT samples (n) are shown on the bottom left side of each figure. The number of ERA5 data is 78,888 data for each figure

with the East Asian winter monsoon are underestimated in the Karimata Strait, Makassar Strait, and Molucca Sea (Figure 7g–i).

We derived major-axis wind components, which are wind components projected onto the major axes of the velocity variance ellipses, to illustrate their relative

frequencies in the selected six locations (Figure 8). The resultant histograms derived from the ERA5 data are consistent with those derived from the ASCAT data, although the slight differences are confirmed only in the Makassar Strait and Molucca Sea due to the different resolution of the datasets. The histograms are bimodal in the locations along the wind route ranging from the Karimata Strait to the Arafura Sea and in the Molucca Sea (Figure 8a,c,d–f). This means that the two peaks are the result of the seasonal reverse of the monsoon wind. The peaks corresponding to the Australian winter monsoon are more dominant than the East Asian winter monsoon, especially in the Java Sea, Banda Sea, and Arafura Sea. The following previous studies discussed the possible factors, which intensify and weaken the East Asian winter monsoon and the Australian winter monsoon. The position and intensity of the Hadley circulation affect the East Asian winter monsoon (Zhang and Zhang, 2010). Chen *et al*. (2019) found that the intensification of the Australian high is favourable for the strengthening of the Australian winter monsoon. In the Makassar Strait, the histogram is monomodal (Figure 8b). This result indicates that the Makassar Strait is a minor route of the monsoons and that the resulting wind speeds are relatively weak. Thus, there are regional differences in the wind speed frequency between the two monsoons.

The monthly averages and standard deviations of the major-axis wind component in the selected six locations were used to respectively investigate the seasonal variations in speed and variability of the monsoon wind (Figure 9). The results derived from both datasets are consistent with each other. The magnitudes of the major-axis wind components during the Australian winter monsoon are larger than those during the East Asian winter monsoon, especially in the Molucca Sea and the Arafura Sea, which are consistent with the aforementioned results (Figures 2, 3, 7, and 8). Another important distinction is that the major-axis wind components exhibit larger variability during the East Asian winter monsoon

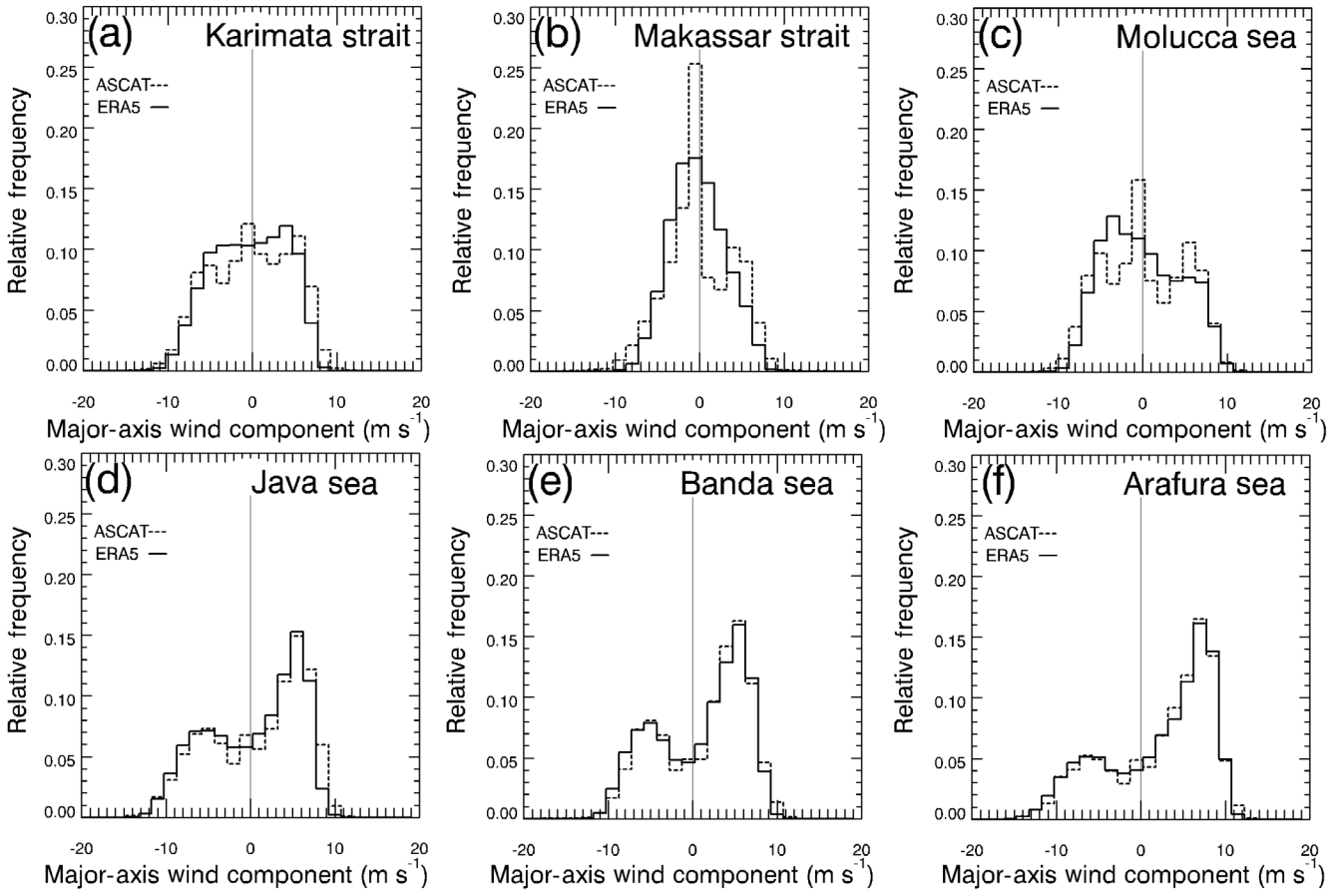

FIGURE 8 Relative frequency of the major-axis wind component in the selected six locations shown in Figure 1b. The ASCAT and hourly data of ERA5 at 10 m are used. We here define the positive direction of the major axis of the velocity variance ellipse as the direction consistent with the mean wind vector during the Australian winter monsoon in Figure 3. The positive and negative values of the major-axis wind component indicate the wind mainly associated with the Australian winter monsoon and the East Asian winter monsoon, respectively. The numbers of ASCAT and ERA5 data used are the same as Figure 7

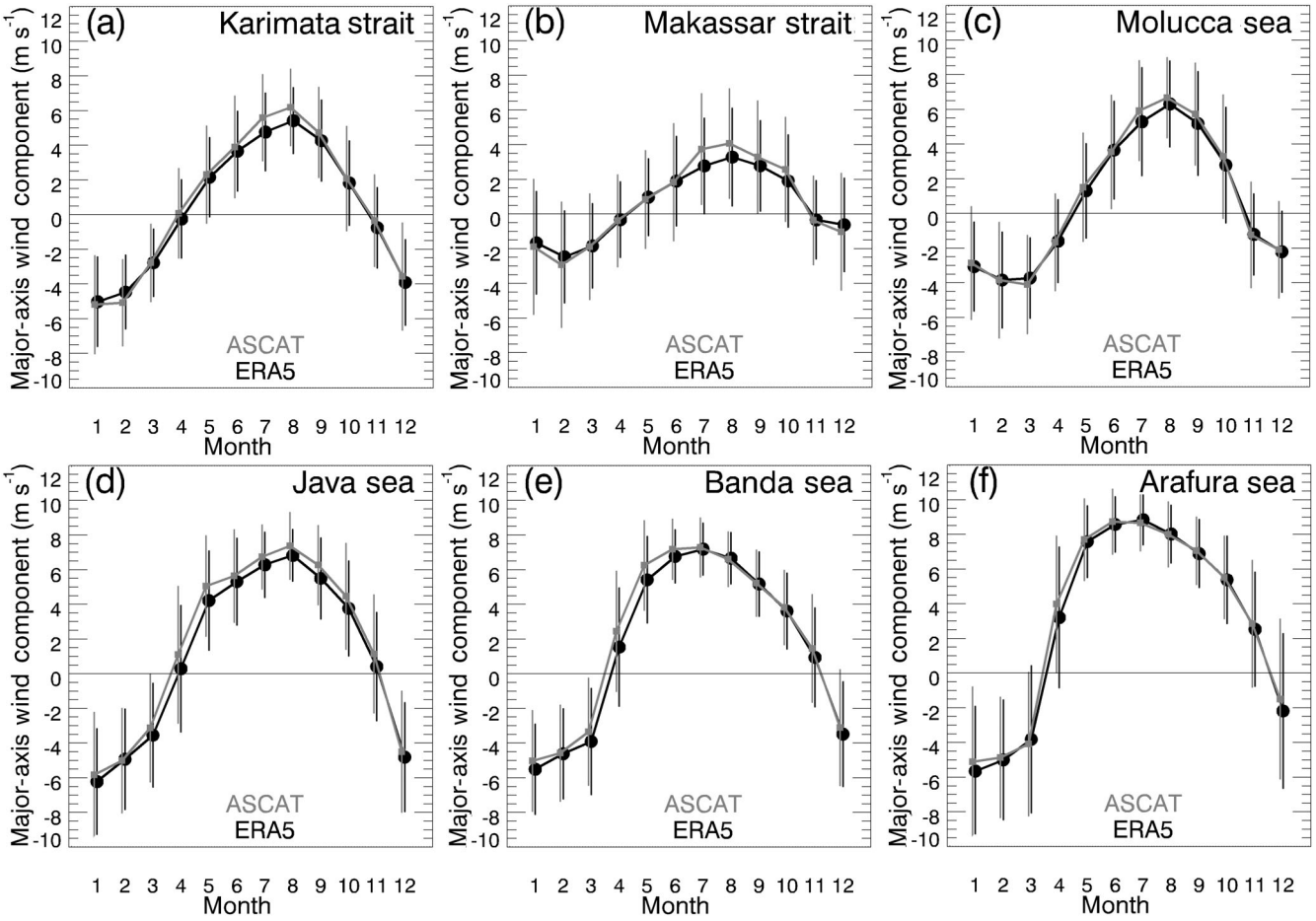

FIGURE 9 Monthly mean (thick lines and dots) and ±1 standard deviation (thin vertical lines) of the major-axis wind component derived from ASCAT (grey) and hourly data of ERA5 at 10 m (black) at a single grid corresponding to the selected six locations in Figure 1b. Positive and negative values of the major-axis wind component represent the winds blowing during the Australian winter monsoon and the East Asian winter monsoon, respectively

than that during the Australian winter monsoon along the route of the monsoon (the Karimata Strait, Java Sea, Banda Sea, and Arafura Sea; Figure 9a,d–f). This distinction is particularly prominent in the Java Sea, Banda Sea, and Arafura Sea (Figure 9d–f). In the Makassar Strait and the Molucca Sea, the variability in the major-axis wind component is comparable between the two monsoons. The large variabilities in the major-axis wind component are evident during the monsoon transitions in the Molucca Sea, Java Sea, Banda Sea, and Arafura Sea (Figure 9c–f). The overall features of the seasonal variations in the Java Sea, Banda Sea, and Arafura Sea are similar to each other (Figure 9d–f), with earlier peaks of the Australian winter monsoon than the other locations (Figure 9a–c). Winds in the Makassar Strait are markedly weaker than the other locations (Figure 9c). These results above clearly exhibit the difference between the two monsoons.

We examined the seasonal advance of the monsoons in the Indonesian seas from the daily means of the major-axis wind component along the main monsoon routes shown in Figure 1b (Figure 10). Although in the results so far, we used both ASCAT and ERA5 data, in this and subsequent analyses, we use the ERA5 data to take advantage of its high temporal resolution. Although the onset and retreat dates of the monsoons have been discussed mainly from rainfall data or wind data in the lower atmosphere (Tanaka, 1994; Moron *et al.*, 2009, 2010), we considered this issue in terms of sea surface winds. In Figure 10, positive and negative values persist for months and divide a year into two seasons. This persistence of the positive and negative values of the major-axis wind component represents the duration of the Australian winter monsoon and theEast Asian winter monsoon periods, respectively. The switch between the positive and negative values or the major-axis wind component of 0 m s^{-1} means the transition between the monsoons. The Australian winter monsoon starts from the Arafura Seas at the end of March. The duration of the Australian winter monsoon decreases with distance from

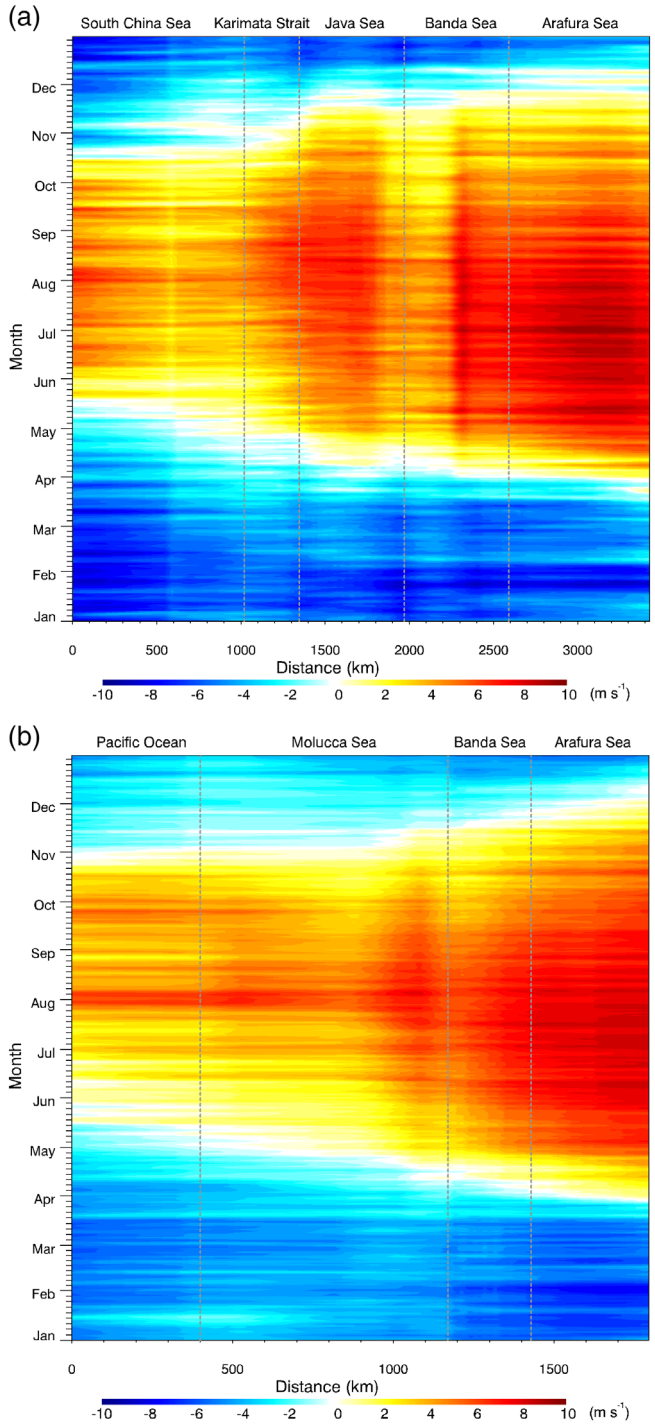

FIGURE 10 Distance-time diagrams of the daily mean of the major-axis wind component along the main monsoon routes denoted by the dashed grey lines in Figure 1b. The ERA5 hourly data at 10 m are used. The defined routes extend to the Arafura Sea from (a) the South China Sea and (b) the Pacific Ocean. Along these routes, the data are sampled at every 0.25° in longitude or latitude and the numbers of sampling locations along the routes are 137 grid points in (a) and 53 grid points in (b). Positive and negative values show the winds blowing during the Australian winter monsoon and the East Asian winter monsoon periods, respectively. The vertical dashed line serves as the only guide of sea boundaries [Colour figure can be viewed at wileyonlinelibrary.com]

the Arafura Sea to the South China Sea (Figure 10a). That is, the Australian winter monsoon has a duration of 7.5 months (from early April to the middle of November) in the Arafura Sea and 5.5 months (from early May to the middle of October) in the South China Sea. The East Asian winter monsoon starts in mid-October in the South China Sea and reaches the Arafura Seas at the beginning of December (Figure 10a). The complete transition between the East Asian winter monsoons and the Australian winter monsoons in the Indonesian seas takes approximately 40 days. Along the route extending from the Arafura Sea to the Pacific Ocean (Figure 10b), the overall features are common to those in Figure 10a. In the Pacific Ocean, the transitions from the Australian winter monsoon to the East Asian winter monsoon occur after a delay of a half month (starting at the beginning of November), compared to the South China Sea. Thus, we can see the onset dates and the transition of the monsoons in the Indonesian seas from the wind components along the monsoon routes.

Along the defined routes, we can see the following regional distributions of the major-axis wind component. The Australian winter monsoon has maximum speeds of approximately 10 m s^{-1} only in the Arafura Sea and the Banda Sea (Figure 10a,b). The maximum speeds occur during May–August or the first half of the Australian winter monsoon period. In the boundary region between the Java Sea and the Karimata Strait, the Australian winter monsoon intensifies up to a speed of approximately 8 m s^{-1} in August (Figure 10a). In the Molucca Sea and the Pacific Ocean, the maximum speeds also appear in August (Figure 10b). In contrast, the maximum speeds associated with the East Asian winter monsoon extend far downstream from the Java Sea to the Arafura Sea with comparable speeds (approximately 8 m s^{-1}) to those in the South China Sea (Figure 10a). Moreover, the maximum speeds persist throughout the East Asian winter monsoon. A local minimum of wind speed is found in the Karimata Strait. Along the route from the Pacific Ocean to the Arafura Sea, wind speeds blowing through the Molucca Sea are slightly weaker than those in the Banda Sea and Arafura Sea (Figure 10b). Thus, Figure 10 corroborates the spatial analyses of the monsoon wind in Figures 1–3 in terms of seasonal variations.

5 | DIURNAL VARIATION

The ERA5 hourly wind data were used to analyse the diurnal variation of wind by taking advantage of long-term data and of higher temporal resolution compared to the data used in Short *et al.* (2019). The diurnal variations

of wind derived from the ERA5 data and in situ data show consistency (Figure S2c). The differences in wind speeds between these two datasets are attributed to the observation height of the stations, representativeness of the in situ observation, and the grid interval of ERA5 (Table S1, Figure S2a,b). Furthermore, the comparison between wind speeds obtained from ERA5 and those from the Triangle Trans-Ocean Buoy Network (TRITON) buoys located to the north of Papua show significantly high correlations (>.8) with a mean bias and root mean square less than −0.27 and 1.42 m s^{-1}, respectively (Figure S3). Thus, we conclude that the ERA5 wind data can be effectively used for the analysis of diurnally varying wind in the Indonesian seas.

Figure 11 depicts the result for September when diurnal wind variations are the most prominent in a year, as shown in Figure 13a. The vector wind field in September is similar to that in August (Figure 3a,b) but with slightly lower speeds. The vector anomalies indicate land breezes during the nighttime and sea breezes during the daytime. The wind rapidly changes its direction to be perpendicular to the coastline (Figure 11). This result is consistent with the studies in southwestern Sumatra Island (Arakawa and Kitoh, 2005), in the sea near Borneo and Sulawesi Island (Lang, 2017), in the western Maritime Continent (Lu *et al*., 2019), and in the eight selected transects of the Indonesian seas (Short *et al*., 2019). The land–sea breezes typically propagate over 400 km offshore in the Maritime Continent (Short *et al*., 2019). The wind generally rotates diurnally in a clockwise direction in the Northern Hemisphere and in a counterclockwise direction in the Southern Hemisphere because of the Coriolis effect (Gille *et al*., 2005). These general features of diurnal wind variation are confirmed throughout the year (Figure S4).

The map of the diurnal amplitude clearly shows regional differences in the diurnally varying wind (Figure 12). Amplitudes greater than 1.5 m s^{-1} are found along the northern coasts of Java Island and the small islands to the east, along the northwest, northeast, and southwest coasts of Borneo, along the coast of southern Sulawesi Island, and to the southwest of Papua. The most extensive amplitudes of diurnally varying wind are found in the seas near the northern Australian continent. Sea

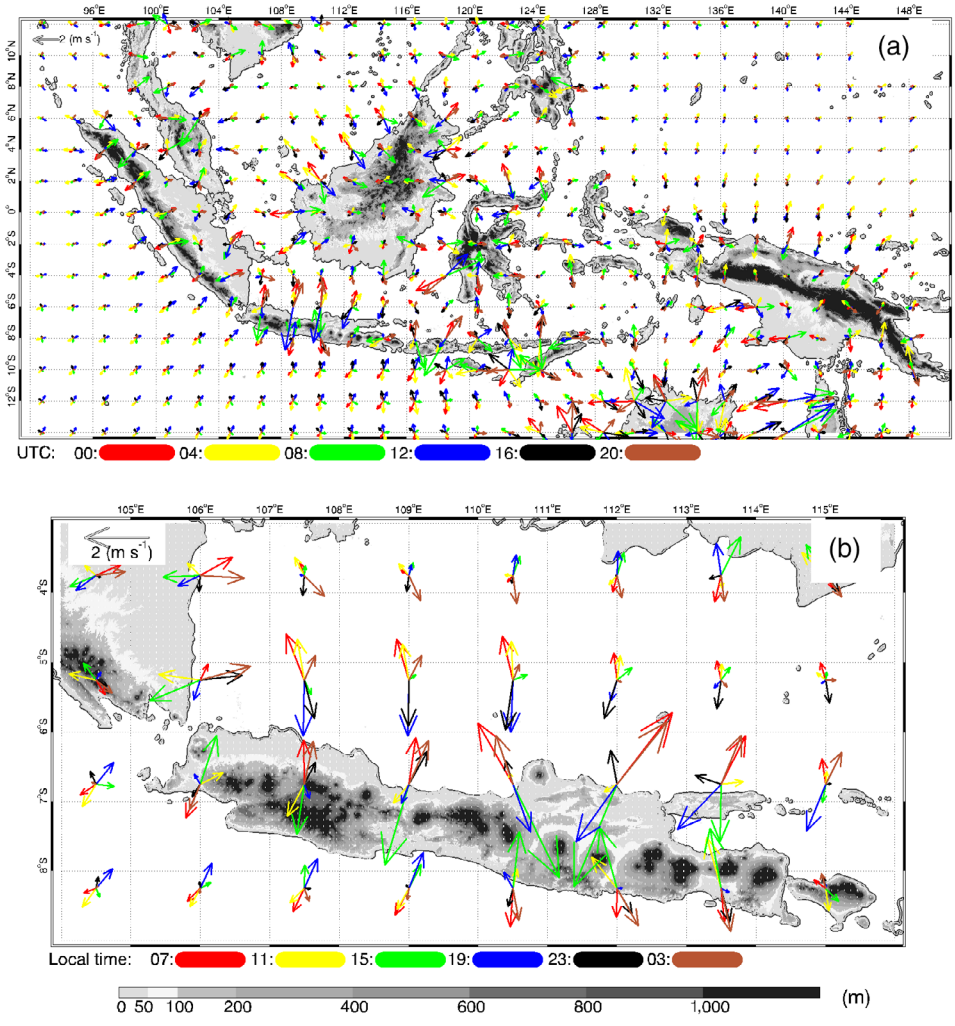

FIGURE 11 (a) Monthly means of anomaly vectors of hourly wind in September from the ERA5 hourly data at 10 m. The colours of the vectors indicate UTC. (b) A closeup of (a) around the Java Sea. The colours of the vectors indicate local times in this region. The anomaly vectors are plotted every 4 hr [Colour figure can be viewed at wileyonlinelibrary.com]

areas with amplitudes of diurnally varying wind greater than 1.5 m s^{-1} are common throughout the year and asymmetrically formed around the islands. In September, these sea areas are commonly located in the lee of the islands. The diurnal variation of wind is presumably enhanced because of weak winds in the lee of the islands. Moreover, the weak wind contributes to an increase in surface temperature over land, increasing the land-sea temperature difference during the daytime. In contrast, the amplitudes of diurnally varying wind are persistently low along the centre lines of the main monsoon routes extending from the Arafura Sea to the South China Sea and to the Pacific Ocean. This feature is especially prominent around the islands in the Molucca Sea, the Halmahera Sea, and the Banda Sea. Thus, regional differences in the amplitudes of diurnally varying winds are identified.

Figure 13a shows the seasonal variation of the diurnal amplitude of wind in the representative regions shown in Figure 12. In the Java Sea, to the south of Sulawesi Island, and to the southwest of Papua, the amplitudes of diurnally varying wind reach a significant maximum in September, with the amplitude of 1.3–1.6 m s^{-1}. To the northwest of Borneo and to the north of Sulawesi Island, the amplitudes of diurnally varying wind have two moderate maximum peaks of 0.7–1.0 m s^{-1} in April and in November or September. We speculate that these seasonal variations of diurnally varying wind are attributable to the daily maxima of the surface temperature difference between land and sea (Figure 13b). We focus on the regions with amplitudes of diurnally varying wind greater than 1.5 m s^{-1}. The land-sea temperature differences in the Java Sea (Region a), off southern Sulawesi Island (Region b), and off southwestern Papua (Region c) reach a high amplitude (more than 1.8 K) in September, consistent with the peak of wind anomaly. The land surface temperature is mainly higher than the sea surface temperature with a significant peak in September (the Java Sea and off southwestern Papua) and October (off southern Sulawesi Island). In these regions, the land-sea thermal contrast and the seasonal variations in temperature over land and sea exert a significant influence on the amplitude of diurnally varying wind in the Indonesian seas. Meanwhile, off northwestern Borneo (Region d) and off northern Sulawesi Island (Region e), the land surface temperature is mainly lower than sea surface temperature (except from January to March for the northern Borneo). Accordingly, the land-sea surface temperature differences in the northern Borneo and northern Sulawesi Island are mainly lower than those in the Region a–c. This result suggests the presence of other factors contributing to the seasonal variations in the amplitudes of the diurnally varying wind. This point needs to be further explored in future studies.

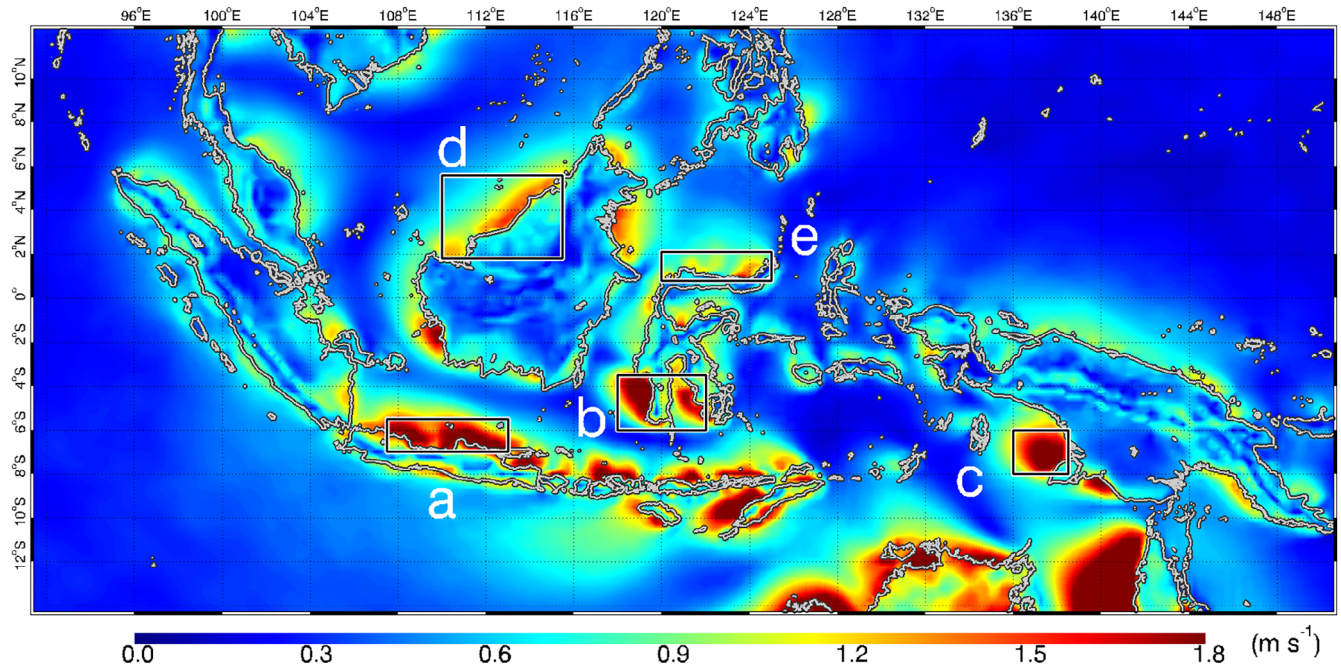

FIGURE 12 Monthly mean of the amplitude of diurnally varying wind in September derived from hourly data of ERA5 at 10 m. Five rectangles with legends of (a–e) show the selected regions for the analyses in Figure 13a [Colour figure can be viewed at wileyonlinelibrary.com]

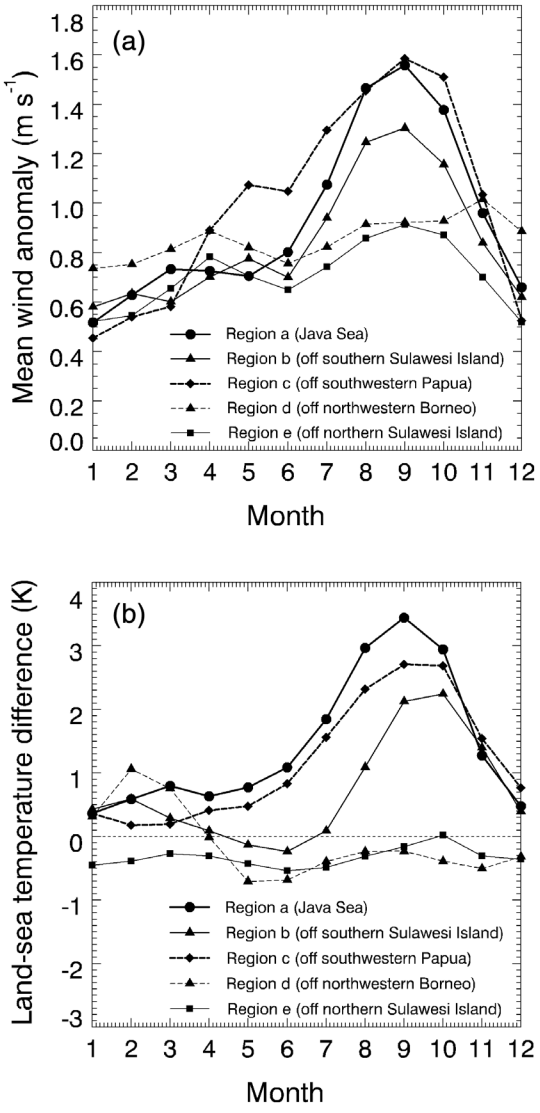

FIGURE 13 (a) Monthly mean amplitudes of diurnally varying wind from ERA5 data at 10 m and (b) monthly variations of daily maxima of the surface temperature difference between land and sea in the five sea regions denoted by the rectangles in Figure 12

6 | SUMMARY AND CONCLUSIONS

This study investigated the surface wind in the Indonesian seas on seasonal and diurnal timescales. The results are summarized as follows:

1. The monsoon winds blow through the Maritime Continent mostly over the seas along the routes formed by the coastline of the large islands and the chains of the small islands. The East Asian winter monsoon blows from the South China Sea to the Arafura Sea through the Karimata Strait, the Java Sea, and the Banda Sea. The trade winds blow into the Banda Sea through the Molucca Sea. The Australian winter monsoon blows mainly from the Arafura Sea to the south of the Philippine Islands or the Pacific Ocean through the Molucca Sea and the Halmahera Sea and partly from the Banda Sea to the South China Sea through the Java Sea. The Makassar Strait also functions as a route for the Australian winter monsoon blowing to the southern Philippine Islands. The wind speeds are persistently strong along these routes. Localized high wind speeds are observed in the Java Sea. The Arafura Sea has the highest wind speed in the Indonesian seas. The wind jets are formed within the routes with high speeds in the central part of the routes, especially in the Java Sea and the Banda Sea. The interisland gaps or channels between the islands also produce wind jets of various scales. Although the Karimata Strait is an important section of the monsoon routes, the structure of the wind jet is not formed. On the other hand, weak winds are formed in the lee of the Philippine Islands, Borneo, and Sulawesi Island owing to the blockage of wind.
2. The major directions of variability in wind are well aligned with the monsoon routes. The monthly mean wind speeds associated with the Australian winter monsoon are higher than those associated with the East Asian winter monsoon in most of the Indonesian seas. Meanwhile, variability in wind associated with the Australian winter monsoon is lower than that associated with the East Asian winter monsoon, especially along the route of the monsoon (the Karimata Strait, the Java Sea, the Banda Sea, and the Arafura Sea). In the Makassar Strait and the Molucca Sea, the variability in wind is comparable between the two monsoon periods. This wind variability shows that the Australian winter monsoon is more persistent than the East Asian winter monsoon. The duration of the Australian winter monsoon is longer than that of the East Asian winter monsoon along the routes ranging from the Java Sea to the Arafura Sea. The onset or retreat date of each monsoon shows a difference of approximately 40 days between the east and west of the Indonesian seas. The Australian winter monsoon exhibits a maximum speed only in the Arafura Sea and the Banda Sea during May–August. The maximum wind speeds associated with the East Asian winter monsoon span a wide range from the Java Sea to the Arafura Sea.
3. The amplitudes of diurnally varying wind are larger along the northern coasts of Java Island and the small islands to the east, along the northwest, northeast, and southwest coasts of Borneo, along the coast of southern Sulawesi Island, and to the southwest of Papua than the other regions near the coast. In the

middle of the seas and along the centre lines of the monsoon routes, the diurnal variation in wind vanishes. Sea areas with a large amplitude of diurnally varying wind are much the same throughout the year. The amplitude of diurnally varying wind has an annual maximum in September, especially in the Java Sea, Banda Sea, and Arafura Sea. These seasonal variations are consistent with the daily maximum temperature differences between land and sea, except in the northern Borneo and northern Sulawesi Island.

We have presented the climatology of surface winds in the Indonesian seas. This study can serve as a basis for a better understanding of weather and climate for the mitigation of disasters. For example, the distribution and intensity of precipitation are essentially affected by surface wind, and thus surface wind is a key for flood management. Then, the study of surface wind is necessary for the development of offshore wind energy. The surface wind is a significant indicator of low-level wind at a rotor height of wind turbines. Moreover, the understanding of surface winds is essential to examine the ocean environment, including the sea state required for the construction and operation of the offshore wind turbines. Further investigations are required in the following aspects. Firstly, examining the three-dimensional structure of the monsoon winds is an important challenge to clarify the effects of island topography on the wind. Wind curl fields in the Indonesian seas indicate significant impacts of the topography of islands of various sizes on the wind. Secondly, regional differences in the amplitude of diurnally varying wind merit further study. Specifically, the cause for the seasonal variations in the amplitude of diurnally varying wind must be investigated. Thirdly, we need to clarify the relationship between the variability of surface winds in the Indonesian seas and the variability of large-scale monsoon systems. The impact of large-scale climate variability induced by ENSO, IOD, and MJO on the surface winds also merits further studies. Further studies along these lines would provide better insights into the formation of the main monsoon routes and the variability in wind on the diurnal to interannual time scales.

ACKNOWLEDGEMENTS

The data of ASCAT onboard MetOp-A and MetOp-B are available from https://podaac.jpl.nasa.gov/dataset/ASCATA-L2-Coastal and https://podaac.jpl.nasa.gov/dataset/ASCATB-L2-Coastal, respectively. The ERA5 reanalysis data were obtained from https://cds.climate.copernicus.eu/cdsapp#!/dataset/reanalysis-era5-single-levels?tab=form. The wind observation data were downloaded from https://www.ncei.noaa.gov/access/search/data-search/global-hourly. The buoy data were obtained from the Global Tropical Moored Buoy Array (GTMBA) Project of NOAA/PMEL (https://www.pmel.noaa.gov/tao/drupal/flux/index.html). The first author would like to acknowledge the INPEX Scholarship Foundation Japan for supporting this study. The third author would like to thank the Postdoctoral/sabbatical program provided by the World Class University Program of Diponegoro University for promoting this study.

ORCID

Inovasita Alifdini https://orcid.org/0000-0002-5486-5726
Teruhisa Shimada https://orcid.org/0000-0002-5988-7123
Anindya Wirasatriya https://orcid.org/0000-0003-1030-5126

REFERENCES

Ahmed, T., Mekhilef, S., Shah, R., Mithulananthan, N., Seyedmahmoudian, M. and Horan, B. (2017) ASEAN power grid: a secure transmission infrastructure for clean and sustainable energy for South-East Asia. *Renewable and Sustainable Energy Reviews*, 67, 1420–1435. https://doi.org/10.1016/j.rser.2016.09.055.

Aldrian, E. and Susanto, R.D. (2003) Identification of three dominant rainfall regions within Indonesia and their relationship to sea surface temperature. *International Journal of Climatology*, 23, 1435–1452. https://doi.org/10.1002/joc.950.

Arakawa, O. and Kitoh, A. (2005) Rainfall diurnal variation over the Indonesian Maritime Continent simulated by 20 km-mesh GCM. *SOLA*, 1, 109–112. https://doi.org/10.2151/sola.2005-029.

Araki, R., Yamanaka, M.D., Murata, F., Hashiguchi, H., Oku, Y., Sribimawati, T., Kudsy, M. and Renggono, F. (2006) Seasonal and interannual variations of diurnal cycles of wind and cloud activity observed at Serpong, West Jawa, Indonesia. *Journal of the Meteorological Society of Japan*, 84A, 171–194. https://doi.org/10.2151/jmsj.84A.171.

Bhatt, B.C., Sobolowski, S. and Higuchi, A. (2016) Simulation of diurnal rainfall variability over the maritime continent with a high-resolution regional climate model. *Journal of the Meteorological Society of Japan*, 94A, 89–103. https://doi.org/10.2151/jmsj.2015-052.

Chang, C.-P., Harr, P.A. and Chen, H. (2005a) Synoptic disturbances over the equatorial South China Sea and Western Maritime Continent during boreal winter. *Monthly Weather Review*, 133, 489–503. https://doi.org/10.1175/MWR-2868.1.

Chang, C.-P., Wang, Z., McBride, J. and Liu, C. (2005b) Annual cycle of Southeast Asia—Maritime Continent rainfall and the asymmetric monsoon transition. *Journal of Climate*, 18, 287–301. https://doi.org/10.1175/JCLI-3257.1.

Chelton, D.B., Freilich, M.H. and Esbensen, S.K. (2000) Satellite observations of the wind jets off the Pacific Coast of Central America. Part I: case studies and statistical characteristics. *Monthly Weather Review*, 128, 1993–2018. https://doi.org/10.1175/1520-0493(2000)128<1993:SOOTWJ>2.0.CO;2.

Chelton, D.B., Schlax, M.G., Freilich, M.H. and Milliff, R.F. (2004) Satellite measurements reveal persistent small-scale features in

ocean winds. *Science*, 303, 978–983. https://doi.org/10.1126/science.1091901.

Chen, W., Guan, Z., Xu, Q. and Yang, H. (2019) Variation of anomalous convergence around Kalimantan Island in lower troposphere and its role in connecting the East Asian summer monsoon and Australian winter monsoon. *Journal of Geophysical Research: Atmospheres*, 124, 6892–6903. https://doi.org/10.1029/2018JD030215.

Copernicus Climate Change Service (C3S) (2017) ERA5: fifth generation of ECMWF atmospheric reanalyses of the global climate. Copernicus Climate Change Service Climate Data Store (CDS). Available at: https://cds.climate.copernicus.eu/cdsapp#!/home.

EMD International A/S. (2017) Wind energy resources of Indonesia Available at: http://indonesia.windprospecting.com/.

EUMETSAT/OSI SAF (2010) MetOp-A ASCAT level 2 ocean surface wind vectors optimized for coastal ocean. Version Operational/Near-Real-Time. PO.DAAC, CA. Available at: https://podaac.jpl.nasa.gov/dataset/ASCATA-L2-Coastal.

EUMETSAT/OSI SAF. (2013) MetOp-B ASCAT level 2 ocean surface wind vectors optimized for coastal ocean. Version Operational/Near-Real-Time. PO.DAAC, CA. Available at: https://podaac.jpl.nasa.gov/dataset/ASCATB-L2-Coastal.

Fairall, C.W., Bradley, E.F., Rogers, D.P., Edson, J.B. and Young, G. S. (1996) Bulk parameterization of air-sea fluxes for TOGA COARE. *Journal of Geophysical Research*, 101, 3747–3764. https://doi.org/10.1029/95JC03205.

Figa-Saldaña, J., Wilson, J.J.W., Attema, E., Gelsthorpe, R.V., Drinkwater, M.R. and Stoffelen, A. (2002) The advanced scatterometer (ASCAT) on the meteorological operational (MetOp) platform: a follow on for European wind scatterometers. *Canadian Journal of Remote Sensing*, 28, 404–412. https://doi.org/10.5589/m02-035.

Gernaat, D.E.H.J., Vuuren, D.P.V., Vliet, J.V., Sullivan, P. and Arent, D.J. (2014) Global long-term cost dynamics of offshore wind electricity generation. *Energy*, 76, 663–672. https://doi.org/10.1016/j.energy.2014.08.062.

Gille, S.T., Smith, S.G.L. and Statom, N.M. (2005) Global observations of the land breeze. *Geophysical Research Letters*, 32, L05605. https://doi.org/10.1029/2004GL022139.

Gordon, A.L., Susanto, R.D. and Vranes, K. (2003) Cool Indonesian throughflow as a consequence of restricted surface layer flow. *Nature*, 425, 824–828. https://doi.org/10.1038/nature02038.

Hasan, M.H., Mahlia, T.M.I. and Nur, H. (2012) A review on energy scenario and sustainable energy in Indonesia. *Renewable Sustainable Energy Reviews*, 16, 2316–2328. https://doi.org/10.1016/j.rser.2011.12.007.

Hattori, M., Mori, S. and Matsumoto, J. (2011) The cross-equatorial northerly surges over the maritime continent and its relationship to precipitation patterns. *Journal of the Meteorological Society of Japan*, 89A, 27–47. https://doi.org/10.2151/jmsj.2011-A02.

Hersbach, H., Bell, B., Berrisford, P., Hirahara, S., Horányi, A., Muñoz-Sabater, J., Nicolas, J., Peubey, C., Radu, R., Schepers, D., Simmons, A., Soci, C., Abdalla, S., Abellan, X., Balsamo, G., Bechtold, P., Biavati, G., Bidlot, J., Bonavita, M., Chiara, G.D., Dahlgren, P., Dee, D., Diamantakis, M., Dragani, R., Flemming, J., Forbes, R., Fuentes, M., Geer, A., Haimberger, L., Healy, S., Hogan, R.J., Hólm, E., Janisková, M., Keeley, S., Laloyaux, P., Lopez, P., Lupu, C., Radnoti, G., Rosnay, P.D., Rozum, I., Vamborg, F., Villaume, S. and Thépaut, J.-N. (2020) The ERA5 global reanalysis. *Quarterly Journal of the Royal Meteorological Society*, 146, 1999–2049. https://doi.org/10.1002/qj.3803.

Ichikawa, H. and Yasunari, T. (2006) Time–space characteristics of diurnal rainfall over Borneo and surrounding oceans as observed by TRMM-PR. *Journal of Climate*, 19, 1238–1260. https://doi.org/10.1175/JCLI3714.1.

Iskandar, I., Rao, S.A. and Tozuka, T. (2009) Chlorophyll-a bloom along the southern coasts of Java and Sumatra during 2006. *International Journal of Remote Sensing*, 30, 663–671. https://doi.org/10.1080/01431160802372309.

Jiang, G., Wei, J., Malanotte-Rizzoli, P., Li, M. and Gordon, A.L. (2019) Seasonal and interannual variability of the subsurface velocity profile of the Indonesian Throughflow at Makassar Strait. *Journal of Geophysical Research: Oceans*, 124, 9644–9657. https://doi.org/10.1029/2018JC014884.

Jourdain, N.C., Gupta, A.S., Taschetto, A.S., Ummenhofer, C.C., Moise, A.F. and Ashok, K. (2013) The Indo-Australian Monsoon and its relationship to ENSO and IOD in reanalysis data and the CMIP3/CMIP5 simulations. *Climate Dynamics*, 41, 3073–3102. https://doi.org/10.1007/s00382-013-1676-1.

Juneng, L. and Tangang, F.T. (2005) Evolution of ENSO-related rainfall anomalies in Southeast Asia region and its relationship with atmosphere–ocean variations in the Indo-Pacific sector. *Climate Dynamics*, 25, 337–350. https://doi.org/10.1007/s00382-005-0031-6.

Koseki, S., Koh, T.-Y. and Teo, C.-K. (2013) Effects of the cold tongue in the South China Sea on the monsoon, diurnal cycle, and rainfall in the Maritime Continent. *Quarterly Journal of the Royal Meteorological Society*, 139, 1566–1582. https://doi.org/10.1002/qj.2052.

Kumar, S.V.V.A., Nagababu, G. and Kumar, R. (2019) Comparative study of offshore winds and wind energy production derived from multiple scatterometers and met buoys. *Energy*, 185, 599–611. https://doi.org/10.1016/j.energy.2019.07.064.

Lang, T.J. (2017) Investigating the seasonal and diurnal cycles of ocean vector winds near The Philippines using RapidScat and CCMP. *Journal of Geophysical Research: Atmospheres*, 122, 9668–9684. https://doi.org/10.1002/2017JD027516.

Lu, J., Li, T. and Wang, L. (2019) Precipitation diurnal cycle over the Maritime Continent modulated by the MJO. *Climate Dynamics*, 53, 6489–6501. https://doi.org/10.1007/s00382-019-04941-8.

Luo, B. and Minnett, P.J. (2020) Evaluation of the ERA5 sea surface skin temperature with remotely sensed shipborne marine-atmospheric emitted radiance interferometer data. *Remote Sensing*, 12, 1873. https://doi.org/10.3390/rs12111873.

Mahmuddin, F. and Hamzah, M.I. (2015) Analysis of ocean wind energy density around Sulawesi and Maluku Islands with scatterometer data. *Energy Procedia*, 65, 107–115. https://doi.org/10.1016/j.egypro.2015.01.041.

Meehl, G.A. and Arblaster, J.M. (2011) Decadal variability of Asian–Australian Monsoon–ENSO–TBO relationships. *Journal of Climate*, 24, 4925–4940. https://doi.org/10.1175/2011JCLI4015.1.

Moron, V., Robertson, A.W. and Boer, R. (2009) Spatial coherence and seasonal predictability of monsoon onset over Indonesia. *Journal of Climate*, 22, 840–850. https://doi.org/10.1175/2008JCLI2435.1.

Moron, V., Robertson, A.W. and Qian, J. (2010) Local versus regional-scale characteristics of monsoon onset and post-onset rainfall over Indonesia. *Climate Dynamics*, 34, 281–299. https://doi.org/10.1007/s00382-009-0547-2.

Qian, J.H., Robertson, A.W. and Moron, V. (2010) Interactions among ENSO, the monsoon, and diurnal cycle in rainfall variability over Java, Indonesia. *Journal of the Atmospheric Sciences*, 67(11), 3524. https://doi.org/10.1175/2010JAS3348.1.

Qian, J.-H., Robertson, A.W. and Moron, V. (2013) Diurnal cycle in different weather regimes and rainfall variability over Borneo associated with ENSO. *Journal of Climate*, 26, 1772–1790. https://doi.org/10.1175/JCLI-D-12-00178.1.

Ramon, J., Lledó, L., Torralba, V., Soret, A. and Doblas-Reyes, F.J. (2019) What global reanalysis best represents near-surface winds? *Quarterly Journal of the Royal Meteorological Society*, 145, 3236–3251. https://doi.org/10.1002/qj.3616.

Risien, C.M. and Chelton, D.B. (2008) A global climatology of surface wind and wind stress fields from eight years of QuikSCAT scatterometer data. *Journal of Physical Oceanography*, 38, 2379–2413. https://doi.org/10.1175/2008JPO3881.1.

Rivas, M.B. and Stoffelen, A. (2019) Characterizing ERA-Interim and ERA5 surface wind biases using ASCAT. *Ocean Science*, 15, 831–852. https://doi.org/10.5194/os-15-831-2019.

Ronghui, H., Wen, C., Bangliang, Y. and Renhe, Z. (2004) Recent advances in studies of the interaction between the East Asian winter and summer monsoons and the ENSO cycle. *Advances in Atmospheric Sciences*, 21, 407–424. https://doi.org/10.1007/BF02915568.

Setiawan, R.Y., Wirasatriya, A., Hernawan, U., Leung, S. and Iskandar, I. (2019) Spatio-temporal variability of surface chlorophyll-a in the Halmahera Sea and its relation to ENSO and the Indian Ocean dipole. *International Journal of Remote Sensing*, 41, 284–299. https://doi.org/10.1080/01431161.2019.1641244.

Shimada, T. (2010) Structures and seasonal variations of surface winds blowing through the Tsushima Strait. *Journal of Applied Meteorology and Climatology*, 49, 1714–1727. https://doi.org/10.1175/2010JAMC2301.1.

Short, E., Vincent, C.L. and Lane, T.P. (2019) Diurnal cycle of surface winds in the maritime continent observed through satellite scatterometry. *Monthly Weather Review*, 147, 2023–2044. https://doi.org/10.1175/MWR-D-18-0433.1.

Sprintall, J., Gordon, A.L., Wijffels, S.E., Feng, M., Hu, S., Koch-Larrouy, A., Phillips, H., Nugroho, D., Napitu, A., Pujiana, K., Susanto, R.D., Sloyan, B., Yuan, D., Riama, N.F., Siswanto, S., Kuswardani, A., Arifin, Z., Wahyudi, A.J., Zhou, H., Nagai, T., Ansong, J.K., Bourdalle-Badié, R., Chanut, J., Lyard, F., Arbic, B.K., Ramdhani, A. and Setiawan, A. (2019) Detecting change in the Indonesian seas. *Frontiers in Marine Science*, 6, 1–24. https://doi.org/10.3389/fmars.2019.00257.

Susanto, R.D., Ffield, A., Gordon, A.L. and Adi, T.R. (2012) Variability of Indonesian throughflow within Makassar Strait, 2004–2009. *Journal of Geophysical Research*, 117(C9), C09013. https://doi.org/10.1029/2012JC008096.

Susanto, R.D., Moore, T.S. and Marra, J. (2006) Ocean color variability in the Indonesian Seas during the SeaWiFS era. *Geochemistry, Geophysics, and Geosystem*, 7, Q05021. https://doi.org/10.1029/2005GC001009.

Tanaka, M. (1994) The onset and retreat dates of the austral summer monsoon over Indonesia, Australia, and New Guinea. *Journal of the Meteorological Society of Japan*, 72, 255–267. https://doi.org/10.2151/jmsj1965.72.2_255.

Vincent, C.L. and Lane, T.P. (2017) A 10-year austral summer climatology of observed and modeled intraseasonal, mesoscale, and diurnal variations over the Maritime Continent. *Journal of Climate*, 30, 3807–3828. https://doi.org/10.1175/JCLI-D-16-0688.1.

Wang, B., Wu, Z., Chang, C., Liu, J., Li, J. and Zhou, T. (2010) Another look at interannual-to-interdecadal variations of the East Asian winter monsoon: the northern and southern temperature modes. *Journal of Climate*, 23, 1495–1512. https://doi.org/10.1175/2009JCLI3243.1.

Wirasatriya, A., Sugianto, D.N., Helmi, M., Setiawan, R.Y. and Koch, M. (2019) Distinct characteristics of SST variabilities in the Sulawesi Sea and the northern part of the Maluku Sea during the southeast monsoon. *IEEE Journal of Selected Topics in Applied Earth Observations and Remote Sensing*, 12, 1763–1770. https://doi.org/10.1109/JSTARS.2019.2913739.

Wu, Q. and Chen, G. (2015) Validation and intercomparison of HY-2A/MetOp-A/Oceansat-2 scatterometer wind products. *Chinese Journal of Oceanology and Limnology*, 33, 1181–1190. https://doi.org/10.1007/s00343-015-4160-4.

Xu, J. (2014) Change of Indonesian Throughflow outflow in response to East Asian Monsoon and ENSO activities since the Last Glacial. *Science China Earth Sciences*, 57, 791–801. https://doi.org/10.1007/s11430-014-4845-0.

Xu, J. and Chan, J.C. (2001) The role of the Asian–Australian Monsoon system in the onset time of El Niño events. *Journal of Climate*, 14, 418–433. https://doi.org/10.1175/1520-0442(2001)014<0418:TROTAA>2.0.CO;2.

Zhang, C. (2013) Madden-Julian oscillation: bridging weather and climate. *Bulletin of the American Meteorological Society*, 94, 1849–1870. https://doi.org/10.1175/BAMS-D-12-00026.1.

Zhang, C. and Zhang, H. (2010) Potential impacts of East Asian winter monsoon on climate variability and predictability in the Australian summer monsoon region. *Theoretical and Applied Climatology*, 101, 161–177. https://doi.org/10.1007/s00704-009-0246-2.

SUPPORTING INFORMATION

Additional supporting information may be found online in the Supporting Information section at the end of this article.

How to cite this article: Alifdini I, Shimada T, Wirasatriya A. Seasonal distribution and variability of surface winds in the Indonesian seas using scatterometer and reanalysis data. *Int J Climatol*. 2021;1–19. https://doi.org/10.1002/joc.7101